Int. J. Solids Structures Vol. 30, No. 5, pp. 637–650, 1993
Printed in Great Britain

0020–7683/93 $6.00+ .00
Pergamon Press Ltd

CONTACT OF ISOTROPIC SQUARE PLATES WITH RIGID SPHERICAL INDENTORS

CHUN-FU CHEN and DANIEL FREDERICK
Department of Engineering Science and Mechanics,
Virginia Polytechnic Institute and State University, Blacksburg, VA 24061, U.S.A.

(*Received* 5 *December* 1991; *in revised form* 2 *September* 1992)

Abstract—The contact problem of an isotropic square plate indented by a rigid spherical indentor was studied. Employing an exact solution method with a simple discretization technique, the numerical sensitivity due to the ill-posed nature of the problem was precluded by enhancing the numerical procedure with a least square technique. For small indentations, the results were compared with the published solutions for a circular plate and good agreement was obtained. Depending upon the size of contact, the contact area was found to be either a circle or a hypotrocoid of four lobes featuring a shorter length of contact along the through-the-corner directions of the plate. The range of applicability of Hertz's theory was found to be limited to very small indentations. The distributions of the contact stresses over the plane of the plate were presented to illustrate the difference of contact behavior between a square plate and a circular plate. The load–indentor displacement relation was presented which showed that a square plate was stiffer than a circular plate under indentation.

NOMENCLATURE

σ_{ij} $(i,j=1,2,3)$	stress components
u_i $(i=1,2,3)$	displacement components
U_i $(i=1,2,3)$	displacement functions
L	side length of the plate
c	semi-contact length
h	thickness of the plate
R	radius of curvature of the indentor
v	Poisson's ratio
λ, μ	Lamé's constants
$f(x,y)$	unknown contact stress
K	number of divisions on c
C_a	$\lambda+2\mu$
C_b	$\lambda+\mu$
r_s, t	hypotrocoidal parameters
C_k	t/r_s
f_{kl}	uniform sub-load
A_{kl}	sub-area for f_{kl}
T_{nm}	Fourier coefficients for f_{kl}
p	$n\pi/L$
q	$m\pi/L$
r	$\sqrt{p^2+q^2}$
a_{ij} $(i,j=1,2,\ldots,6)$	coefficients for U_j
C_α	$(\lambda+3\mu)/(\lambda+\mu)$
Z_i $(i=1,2,\ldots,6)$	defined in eqns (21), (22)
B_α $(\alpha=a,b,\ldots,e)$	defined in eqns (23), (24)
g_a, g_b	defined in eqns (23)
C_+	cosh $(rh/2)$
S_+	sinh $(rh/2)$
H_T	S_+/C_+
H_C	C_+/S_+
K_T, K_C, k_a, k_b	defined in eqns (26)
U_{3t}	U_3 on the top surface
k_c, k_d	defined in eqns (27)
$(u_3)_0$	u_3 at $(L/2, L/2)$
$(u_3)_{ij}$	u_3 at (x_i, y_j)
$(u_3)_{0,kl}$	$(u_3)_0$ due to f_{kl}
$(u_3)_{ij,kl}$	$(u_3)_{ij}$ due to f_{kl}
P_{kl}	magnitude of f_{kl}
P	total contact load
σ_{ai}	intimated average contact stress, $P/(c\times c)$
$\bar{x}$	$(x-L/2)/c$
$\bar{y}$	$(y-L/2)/c$

$\bar{r}$	$\sqrt{(\bar{x}^2+\bar{y}^2)}$
Δ	indentor displacement
D	bending rigidity.

INTRODUCTION

The objective of this study was to solve a three-dimensional contact problem between an isotropic square plate and a rigid spherical indentor within the framework of linear elasticity. Various areas of contact, similar to those employed in the published literature, were considered. Emphasis was placed on demonstrating that the asymmetric finite boundary conditions strongly influence the local contact behavior. In all cases, the primary task in the solution procedure was the determination of the correct contact area in order that the correct contact stresses could be found.

Numerous conformal and counter-formal contact problems simulating wheel/rail contact (Kalker, 1979, 1980a) have been studied. Many numerical algorithms have been developed to determine the correct contact area for various contact geometries. For example, Singh and Paul (1974) posed the problem with a prescribed interpenetration. The numerical sensitivities which arose in their solution were overcome by using RFP (Redundant Field Points) and FR (Functional Regularization) methods. Paul and Hashemi (1979, 1980a) presented an improved numerical method to preclude the occurrence of numerical sensitivity by posing the problem with a known applied load. A technique involving flexibility of analysis was employed by Hartnett (1980) to treat counter-formal contact problems. It was extended by Ahmadi *et al.* (1983) to solve non-Hertzian normal (1980b, 1981, 1983), Duffek (1983) and Duffek and Jaschinski (1981). However, most of the aforementioned approaches were based on using Boussinesq force–displacement relations.

Recently, contact problems involving beams and plates have been increasingly studied. For example, beam problems were solved by Keer and Miller (1983b), Sankar and Sun (1983), Keer and Ballarini (1983) and Sun and Sankar (1985). The case of a cantilever beam was studied by Keer and Schonberg (1986). In these studies, the ratio of contact width to beam thickness, c/h, was treated as a known value, i.e. the problem was posed in a manner different from that employed by Paul and Hashemi (1979, 1980b), Hartnett (1980) and Ahmadi *et al.* (1983). A circular plate indented by a rigid spherical indentor was studied by Keer and Miller (1983a) by considering a similar ratio (c = radius of the contact area). The corresponding impact problem was studied by Schonberg *et al.* (1987). This was further extended to the transversely isotropic case by Schonberg *et al.* (1987). All of these studies revealed non-Hertzian type behavior for large indentations. In contrast to the case of wheel/rail contact, these studies did not lack the knowledge of the shape of the contact area due to planar or axisymmetric considerations. However, in order to satisfy the boundary support conditions, their approach required more algebraic and numerical effort than simply applying the Boussinesq force–displacement relation mentioned earlier.

This study employed the same way of posing the problem as that used by Keer and Miller (1983a) but did not employ the axial symmetry in order to consider a square plate. Friction between the plate and the indentor was neglected. The intention was to investigate the local contact behavior for the case of asymmetric finite boundaries and for the case of large contact areas. The approach extended the simple discretization method presented by Sankar and Sun (1983) to three dimensions. Thus, a candidate contact area was proposed for a prescribed contact length in an in-plane direction. It was discretized along both in-plane directions in order to define various uniform sub-loads over each sub-area in the contact region for the purpose of approximating the unknown contact stress. The displacement fields due to the sub-loads were solved by modifying Pagano's (1970) method for obtaining exact solutions for rectangular plates, rather than superposing a plate theory and an elasticity solution as employed by Keer and Miller (1983a). The form obtained for the displacement was neater than that obtained by applying Pagano's approach (1970) directly. Meanwhile, Chen's (1991) method of detecting terms was utilized in a three-dimensional manner to carry out an efficient series calculation and to save CPU time. Next,

the point matching technique of Sankar and Sun (1983), strengthened by the Redundant Field Point method of Singh and Paul (1974), was used to solve for the magnitudes of various sub-loads and to preclude the possibility of numerical sensitivity. The candidate approximate solution obtained for the unknown contact stress was then checked to see if the stresses were all compressive, a requirement due to the smooth indentation of the problem. Improved candidate contact areas were proposed until this condition was fulfilled. Emphasis was placed upon locating the correct contact area and the associated contact stresses for various lengths of contact in the plane of the plate. The shape of the contact area, although unknown, is of major concern; however, in general it can be reasonably expected to be a circle for relatively small indentations. The limits of validity of both the circular contact area and the Hertzian type solution were studied. The directional-dependence of the contact stress distribution was presented to illustrate the distinction of the present results from those for the circular plate (Keer and Miller, 1983a). The load–indentor displacement relation was studied as well and compared with the circular plate case. The present study excluded any consideration of material anisotropy. Knowledge of the effect of the boundary support conditions upon both the contact surface and the structural behavior are of such fundamental and practical importance that they should be studied prior to considering material anisotropy. The present study thus served as a fundamental study of the three-dimensional contact or impact problem incorporating both material isotropy and boundary condition of plates with finite dimensions.

PROBLEM FORMULATION

An isotropic square plate is considered, as shown in Fig. 1. It is simply supported on all edges in such a manner that only normal displacement but no tangential displacement is allowed along each edge. The plate is indented by a rigid sphere at the center of the top surface without considering the friction between them. Both the domain of the contact region, $Q(x,y)$, and the contact stresses, $f(x,y)$, under the indentor are to be determined. The contact length along the x-axis, c, is assumed to be a known value. The boundary conditions in the through-the-thickness direction are

$$\sigma_{33}\left(x,y,\frac{-h}{2}\right) = -f(x,y), \quad \text{for } (x,y) \text{ in } Q(x,y), \tag{1}$$

$$\sigma_{33}\left(x,y,\frac{-h}{2}\right) = 0, \quad \text{elsewhere}, \tag{2}$$

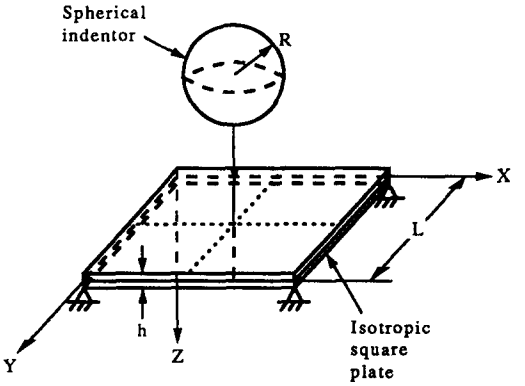

Fig. 1. Isotropic square plate indented by a rigid spherical indentor.

$$\sigma_{31}\left(x, y, \frac{-h}{2}\right) = \sigma_{32}\left(x, y, \frac{-h}{2}\right) = 0, \tag{3}$$

$$\sigma_{33}\left(x, y, \frac{h}{2}\right) = \sigma_{32}\left(x, y, \frac{h}{2}\right) = \sigma_{31}\left(x, y, \frac{h}{2}\right) = 0, \tag{4}$$

$$u_3\left(L/2, L/2, \frac{-h}{2}\right) - u_3\left(x, y, \frac{-h}{2}\right) = \frac{(x-L/2)^2+(y-L/2)^2}{2R}, \quad (x,y) \text{ in } Q(x,y), \tag{5}$$

where h and L are the thickness and the edge length of the plate respectively, and R is the radius of curvature of the indentor. Furthermore, the simply-supported edge conditions require

$$\sigma_{11} = u_2 = u_3 = 0, \quad \text{for } x = 0, L, \tag{6}$$

$$\sigma_{22} = u_1 = u_3 = 0, \quad \text{for } y = 0, L. \tag{7}$$

METHOD OF SOLUTION

Composition/discretization of candidate contact area

Extending Sankar and Sun's approach (1983) to solve the present problem, a candidate contact area will be proposed for a prescribed magnitude of half contact length, c, along the x-axis. This area is discretized along both the x and y directions using the non-uniform discretization scheme (Chen, 1991) to obtain a finer cut close to the contact boundary. By symmetry, only a quarter contact region is displayed as shown in Fig. 2 and a loading factor of 4 is imbedded. In this manner, the candidate contact area is approximated by a polygonal region composed of various sub-areas which can be labelled as follows

$$A_{kl} = 4(x_{k+1}-x_1)(y_{l+1}-y_1), \quad k+l \neq K+1, \tag{8}$$

$$A_{1K} = A_{1(K-1)} + 2(x_2-x_1)(y_{K+1}-y_K), \quad A_{K1} = A_{(K-1)1} + 2(y_2-y_1)(x_{K+1}-x_K), \tag{9}$$

$$A_{k(K+1-k)} = A_{k(K-k)} + 2(x_k+x_{k+1}-2x_1)(y_{K+2-k}-y_{K+1-k}); \quad k = 2, 3, \ldots, K-1, \tag{10}$$

where $k = 1, 2, \ldots, K$; $l = 1, 2, \ldots, K-k+1$ and K is the number of divisions made on c. Thus, the sub-area is either a rectangle if $k+l \neq K+1$ or a trapezoid if $k+l = K+1$.

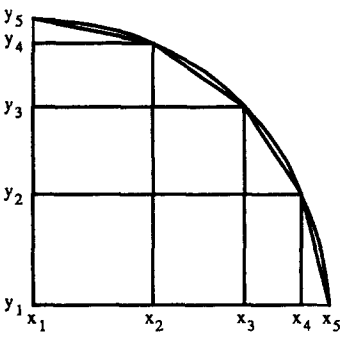

Fig. 2. Discretization of a proposed contact area.

Response due to a typical sub-load

Consider a typical sub-load, f_{kl}, uniformly distributed over the corresponding sub-area A_{kl}. Based on Pagano's approach (1970), the boundary conditions (6) and (7) are satisfied by taking the load, f_{kl}, and the displacement components u_i $(i = 1, 2, 3)$ in the form

$$f_{kl} = \sum_{n=1}^{\infty} \sum_{m=1}^{\infty} T_{nm} \sin(px) \sin(qy), \tag{11}$$

$$u_1 = U_1(z) \cos(px) \sin(qy), \quad u_2 = U_2(z) \sin(px) \cos(qy),$$
$$u_3 = U_3(z) \sin(px) \sin(qy), \tag{12}$$

where U_j $(j = 1, 2, 3)$ are functions of z only, the T_{nm}s are the Fourier coefficients, and $p = n\pi/L$ and $q = m\pi/L$. The T_{nm}s for the various sub-loads are defined in the Appendix while the expressions for U_j $(j = 1, 2, 3)$ were given by Pagano (1970) in terms of exponential functions. These expressions are modified here using the hyperbolic functions, i.e.

$$U_i = (a_{1i} + a_{3i}z + a_{5i}z^2)C_h + (a_{2i} + a_{4i}z + a_{6i}z^2)S_h, \tag{13}$$

where $i = 1, 2, 3$ and a_{ji} $(j = 1, 2, \ldots, 6)$ are unknown constants to be determined. In addition, $C_h = \cosh(rz)$, $S_h = \sinh(rz)$ and $r = \sqrt{p^2 + q^2}$. Of the 18 constants, a_{ji}, only six are independent. Various relations among the a_{ij}s can be deduced to be (Chen, 1991)

$$a_{5j} = a_{6j} = 0 \,(j = 1, 2, 3), \quad a_{(2+i)2} = \frac{q}{p} a_{(2+i)1} \,(i = 1, 2), \quad \begin{bmatrix} a_{43} \\ a_{33} \end{bmatrix} = \frac{r}{p} \begin{bmatrix} a_{31} \\ a_{41} \end{bmatrix}, \tag{14}$$

$$\begin{bmatrix} a_{13} \\ a_{23} \end{bmatrix} = \frac{1}{r} \left\{ p \begin{bmatrix} a_{21} \\ a_{11} \end{bmatrix} + q \begin{bmatrix} a_{22} \\ a_{12} \end{bmatrix} \right\} - \frac{C_\alpha}{p} \begin{bmatrix} a_{31} \\ a_{41} \end{bmatrix}, \tag{15}$$

where $C_\alpha = (\lambda + 3\mu)/(\lambda + \mu)$, and λ and μ are the Lamé constants. In comparison to Pagano's approach (1970), $a_{5j} = a_{6j} = 0$ $(j = 1, 2, 3)$ are identically obtained. However, the remaining relations are different from those of Pagano's derivations (1970). Here, the independent constants are taken to be a_{ij} $(i, j = 1, 2)$, a_{31}, a_{41}. The expressions for U_js can now be rewritten as

$$U_1 = (a_{11} + za_{31})C_h + (a_{21} + za_{41})S_h, \quad U_2 = \left(a_{12} + z\frac{q}{p}a_{31}\right)C_h + \left(a_{22} + z\frac{q}{p}a_{41}\right)S_h, \tag{16}$$

$$U_3 = \left[\frac{pa_{21} + qa_{22}}{r} - \frac{C_\alpha a_{31} - zra_{41}}{p}\right]C_h + \left[\frac{pa_{11} + qa_{12}}{r} - \frac{C_\alpha a_{41} - zra_{31}}{p}\right]S_h, \tag{17}$$

and the out-of-plane stress components σ_{3j} $(j = 1, 2, 3)$ are found to have the form

$$\sigma_{33} = \{2\mu[p(a_{11}C_h + a_{21}S_h) + q(a_{12}C_h + a_{22}S_h)] + Z_1a_{31} + Z_2a_{41}\} \sin(px) \sin(qy), \tag{18}$$

$$\sigma_{32} = \mu\left\{\frac{pq}{r}(a_{11}S_h + a_{21}C_h) + B_b(a_{12}S_h + a_{22}C_h) + Z_3a_{31} + Z_4a_{41}\right\} \sin(px) \cos(qy), \tag{19}$$

$$\sigma_{31} = \mu\left\{\frac{pq}{r}(a_{12}S_h + a_{22}C_h) + B_d(a_{11}S_h + a_{21}C_h) + Z_5a_{31} + Z_6a_{41}\right\} \cos(px) \cos(qy), \tag{20}$$

where

$$Z_1 = g_a z C_h + B_a S_h, \quad Z_2 = g_a z S_h + B_a C_h, \quad Z_3 = g_b z S_h + B_c C_h, \tag{21}$$

$$Z_4 = g_b z C_h + B_c S_h, \quad Z_5 = 2rz S_h + B_e C_h, \quad Z_6 = 2rz C_h + B_e S_h, \tag{22}$$

$$g_a = \frac{2\mu r^2}{p}, \quad g_b = \frac{2rq}{p}, \quad B_a = (\lambda+2\mu)\frac{r}{p}B_e, \quad B_b = \frac{q^2}{r}+r, \tag{23}$$

$$B_c = \frac{q}{p}B_e, \quad B_d = \frac{p^2}{r}+r, \quad B_e = 1-C_\alpha. \tag{24}$$

For a typical T_{nm}, via the boundary conditions in the thickness direction (1) to (4), the six unknown constants can be solved to be

$$a_{i2} = \frac{q}{p}a_{i1}\ (i=1,2), \quad a_{41} = \frac{-2r}{K_C}a_{11}, \quad a_{31} = \frac{-2r}{K_T}a_{21},$$

$$a_{11} = \frac{-T_{nm}}{4k_a C_+}, \quad a_{21} = \frac{T_{nm}}{4k_b S_+}, \tag{25}$$

where

$$K_T = B_e + rhH_T, \quad K_C = B_e rhH_C, \quad k_a = \frac{r}{p}k_c, \quad k_b = \frac{r}{p}k_d, \tag{26}$$

$$k_c = r\left[\mu - \frac{1}{K_C}(\mu rhH_T + C_a B_e)\right], \quad k_d = r\left[\mu - \frac{1}{K_T}(\mu rhH_C + C_a B_e)\right]. \tag{27}$$

In addition,

$$H_T = \frac{S_+}{C_+}, \quad H_C = \frac{C_+}{S_+}, \quad C_+ = \cosh(rh/2), \quad S_+ = \sinh(rh/2) \quad \text{and} \quad C_a = \lambda+2\mu.$$

Finally, U_3 on the top surface, referred to as U_{3t}, can be expressed as

$$U_{3t} = \frac{T_{nm}}{4}(1+C_\alpha)\left(\frac{H_T}{k_c K_C} + \frac{H_C}{k_d K_T}\right), \tag{28}$$

and the transverse displacement u_3 at (x, y) due to a typical sub-load f_{kl} will be

$$(u_3)_{,kl} = \sum_{n=1}^{\infty}\sum_{m=1}^{\infty} U_{3t}(n,m)\sin(px)\sin(qy). \tag{29}$$

The indentation problem

Having solved for the transverse displacement field on the top surface of the plate due to a typical sub-load f_{kl}, the Point Matching Technique of Sankar and Sun (1983) is employed in a three-dimensional manner to solve for the P_{kl}s, the magnitudes of f_{kl}s. For a point (x_i, y_j) inside the contact area, $Q(x, y)$, the contact relation (5) requires that

$$(u_3)_0 - (u_3)_{ij} = \frac{\left(x_i - \frac{L}{2}\right)^2 + \left(y_j - \frac{L}{2}\right)^2}{2R}, \tag{30}$$

where $(u_3)_0 = u_3$ at $x = y = L/2$, $(u_3)_{ij} = u_3$ at (x_i, y_j), and

$$(u_3)_0 \simeq \sum_{k=1}^{K} \sum_{l=1}^{K-k+1} (u_3)_{0,kl} P_{kl}, \quad (u_3)_{ij} \simeq \sum_{k=1}^{K} \sum_{l=1}^{K-k+1} (u_3)_{ij,kl} P_{kl}, \tag{31}$$

for the case of K divisions made along c. In the above, $(u_3)_{0,kl}$ is $(u_3)_0$ due to f_{kl} and $(u_3)_{ij,kl}$ is $(u_3)_{ij}$ due to f_{kl}. Consequently,

$$\sum_{k=1}^{K} \sum_{l=1}^{K-k+1} [(u_3)_{0,kl} - (u_3)_{ij,kl}] P_{kl} \simeq \frac{\left(x_i - \frac{L}{2}\right)^2 + \left(y_j - \frac{L}{2}\right)^2}{2R}. \tag{32}$$

By taking as many reference points (x_i, y_j) as the total number of the sub-loads, $K(K+1)/2$, a set of simultaneous equations similar to (32) can be constructed to solve for the P_{kl}s. In using this method, however, numerical sensitivity was experienced. To cure the numerical sensitivity, the RFP method of Singh and Paul (1974) was employed. The number of reference points in both the x and y directions was doubled.

NUMERICAL RESULTS AND DISCUSSION

For demonstration and comparison purposes, the solution is implemented for a plate with $L/h = 20$ corresponding to the case of $a/h = 10$ (a = radius) for the circular plate studied by Keer and Miller (1983a). The magnitudes of the ratio c/h considered by Keer and Miller (1983a) will be adopted here, i.e. $c/h = 0.5, 1.0, 2.0, 4.0$. The contact stresses to be presented are normalized by an intimated average contact stress, $\sigma_{Al} = p/(c \times c)$, where P is the total contact load. However, locations in the contact area will be normalized by the semi-contact length c.

For $c = 0.5h$, the contact area is proposed to be a circle with various numbers for K. The contact stresses are found to be all compressive and thus the proposed circular shape for the contact area is correct for such a small indentation. The convergence of the total contact force with respect to K is found to be excellent even for a small number for K, which may be less than 10, as shown in Fig. 3. For $K = 8, 9, 10$, for example, the total contact force is essentially constant. For $K = 10$, the distribution of contact stresses in the y direction for various x locations is shown in Fig. 4. Apparently, the result for this case is close to the Hertzian type behavior and is nearly ellipsoidal in shape. In particular, the curve along $\bar{x} = 0.0$, i.e. the radial direction, is identical to the circular plate result obtained by Keer and Miller (1983a). Thus, the size of the contact in this case is sufficiently small so that the local contact behavior is not affected by the finite boundary of the plate, regardless of its shape. For $c = 1.0h$, a circle is proven to be the true contact shape since the contact

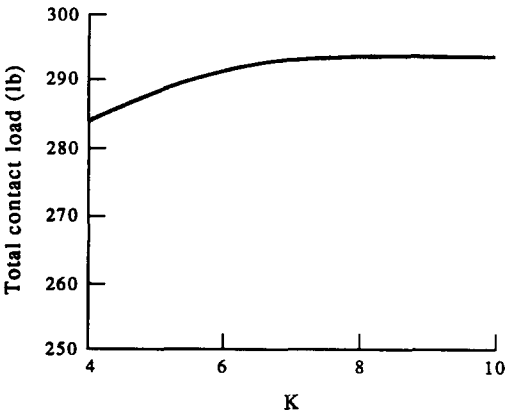

Fig. 3. Total contact load vs K.

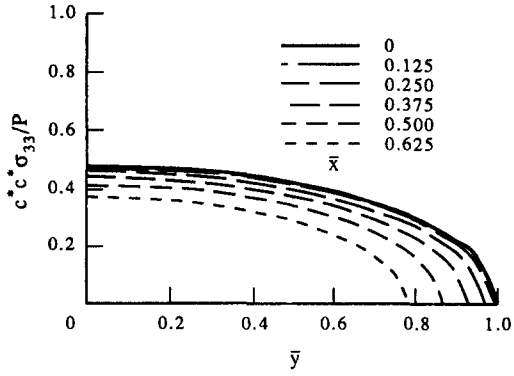

Fig. 4. Contact stress for $c = 0.5h$ (contact area : circle).

stresses are all compressive. As shown in Fig. 5, however, the distribution of contact stresses deviates from the Hertzian type solution but not very appreciably.

For $c = 2.0h$, a three-dimensional contact stress distribution is displayed in Fig. 6 by proposing a circular contact area. A steep jump in the compressive stress arises near the end of the contact lengths in both the x and y directions. However, a small tension is observed in the neighborhood of the contact boundary around the 45° direction. This incorrect candidate solution implies that the contact length along the 45° direction should be reduced or the contact lengths in the x and y directions should be increased comparatively.

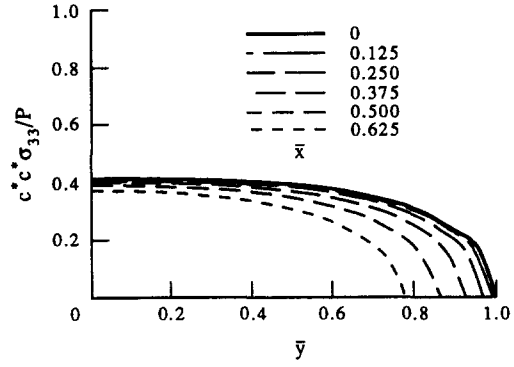

Fig. 5. Contact stress for $c = 1.0h$ (contact area : circle).

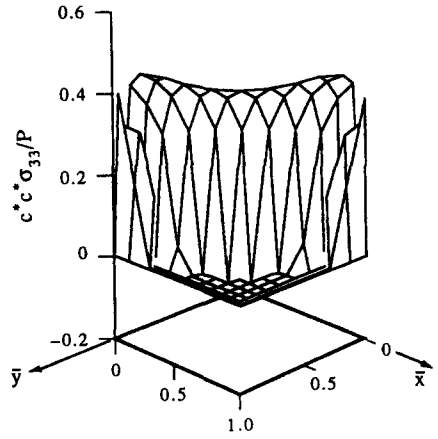

Fig. 6. Contact stress for $c = 2.0h$ (proposed contact area : circle).

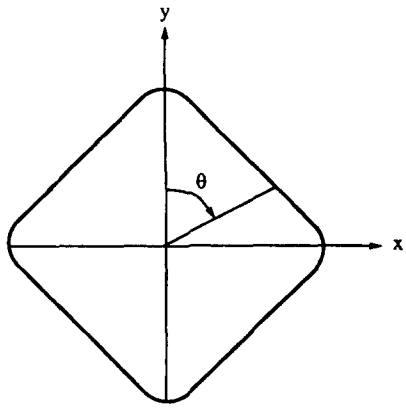

Fig. 7. Typical hypotrocoid of four lobes.

A curve which is not a circular arc but features with such characteristics is a hypotrocoid of four lobes as shown in Fig. 7. It is expressible in terms of the following equations (Holmes, 1978)

$$x = 3r_s \sin(\theta) - t \sin(3\theta), \quad y = 3r_s \cos(\theta) + t \cos(3\theta), \tag{33}$$

where r_s and t, both positive with $0 < t \leqslant r_s$, are the parameters controlling the appearance of the hypotrocoidal curves. For the second attempt, a hypotrocoid curve with $C_k = t/r_s = 0.01$ is considered and is found to produce all compressive contact stresses as illustrated in Fig. 8 for various radial directions with respect to the x-axis. In Fig. 8, $\bar{r} = \sqrt{\bar{x}^2 + \bar{y}^2}$, where $\bar{x} = (x - L/2)/c$ and $\bar{y} = (y - L/2)/c$. Due to isotropy and symmetry, only the directions ranging from 0° to 45° passing through the corners of the plate are included. Apparently, the directional-dependence of the contact stress is marginal. The contact stress distribution in this case deviates significantly from the Hertzian type solution. However, both the peaking of the contact stresses near the contact boundary and the slight wrapping of the plate around the indentor in the central region are similar to those observed by Keer and Miller (1983a).

For a large indentation with $c = 4.0h$, a gradual transition to the correct contact area is demonstrated in Figs 9–12 by proposing $C_k = 0$ (circle), 0.02, 0.04, 0.06 respectively. The greater the parameter, C_k, i.e. the further away from a circle, the smaller the magnitude of the tensile stress. Finally, by taking $C_k = 0.075$, the tension is eliminated. As shown in Fig. 13, the contact stress in this case is extremely non-Hertzian. Wrapping of the plate around the indentor in the center and peaking of the contact stress near the contact boundary are similarly observed and are more severe than in the previous case. In comparison to the case of the circular plate, the size of the region free of contact stress is different. For the square

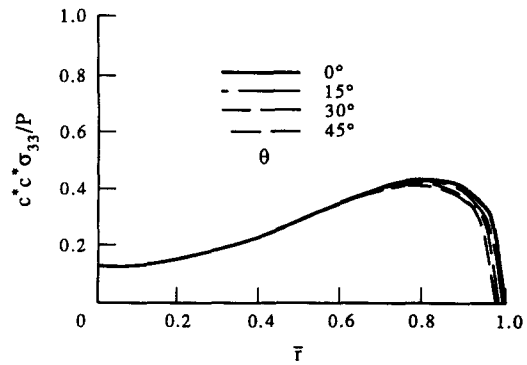

Fig. 8. Contact stress for $c = 2.0h$ (hypotrocoid, $C_k = 0.01$).

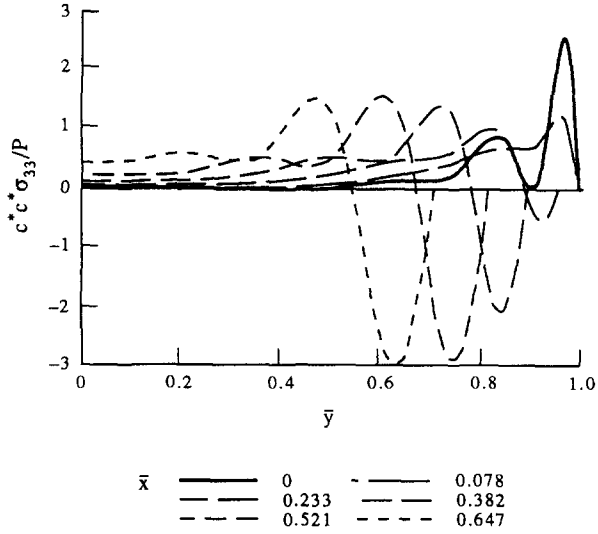

Fig. 9. Contact stress for $c = 4.0h$ (proposed contact area : circle).

plate, from the center to the border of the contact area, the contact stress along any direction rises in magnitude earlier than for the circular plate. Thus, near the center of the contact area, the domain of the region free of contact stress in the square plate is smaller than in the circular plate for this case. In addition, from the center of the contact boundary, the

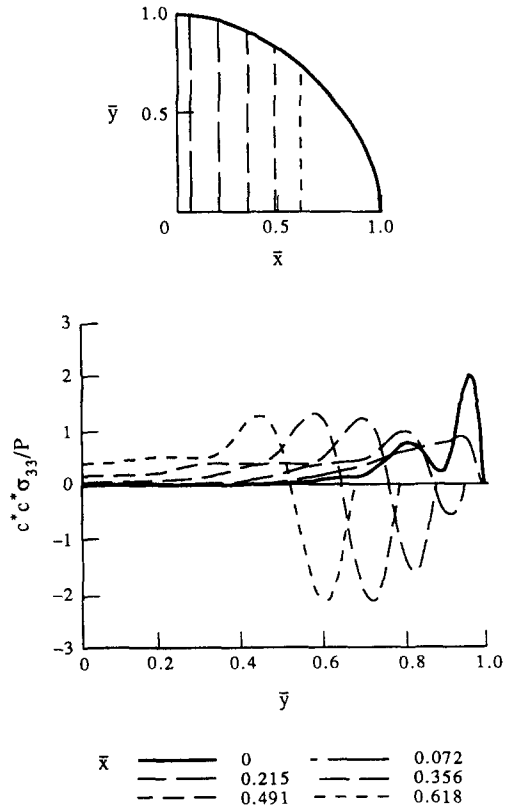

Fig. 10. Contact stress for $c = 4.0h$ (hypotrocoid, $C_k = 0.02$).

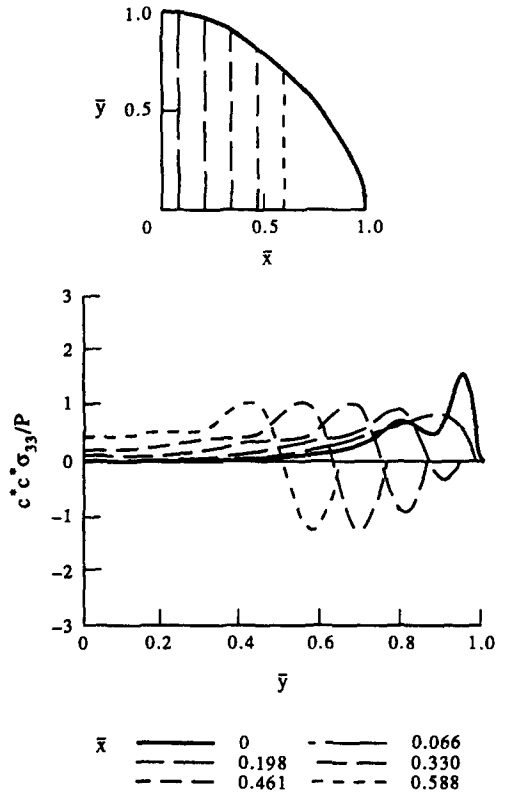

Fig. 11. Contact stress for $c = 4.0h$ (hypotrocoid, $C_k = 0.04$).

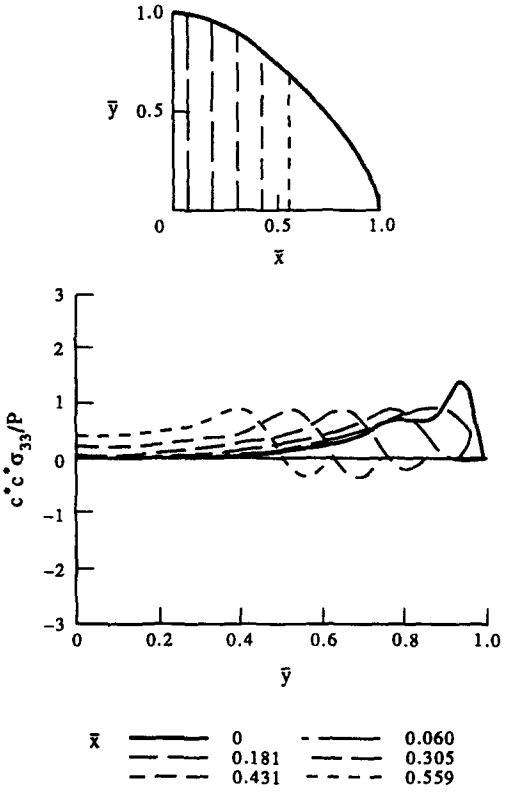

Fig. 12. Contact stress for $c = 4.0h$ (hypotrocoid, $C_k = 0.06$).

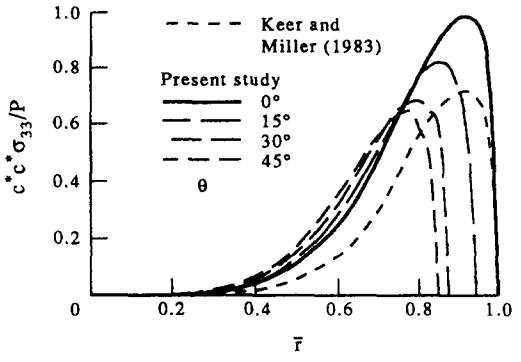

Fig. 13. Contact stress for $c = 4.0h$ (hypotrocoid, $C_k = 0.075$).

contact stress distributions along different directions reach their peak values at different locations with different magnitudes all of which are different from the circular plate result. For $\theta = 0°$, for example, the peak contact stress can be 30% higher than the circular plate result but the locations are nearly the same. Thus, the contact stress in the through-the-mid-span direction of the square plate is distributed wider than in the circular plate. In the 15° direction, the contact length is slightly decreased but the peak value of the contact stress can still be greater than that of the circular plate by 15% and the location is shifted toward the center of indentation. From the 15°- to the 30°-directions, both the maximum contact stress and the contact length are reduced by about the same amounts as those from the 0°- to the 15°-directions. Along both the 30°- and 45°-directions, the contact stresses are distributed over a similarly narrower width and their peak values are found to be smaller than in the circular plate.

Finally, the relation between the total contact load and the indentor displacement is established and shown in Fig. 14. Keer and Miller's solution (1983a) is also included for comparison and their normalization scheme is employed. Clearly, the difference between the two solutions is visible for most of the magnitudes of indentation but is negligible for relatively small indentations. That the curve for the square plate is located above the curve for the circular plate indicates that, in order to have the same amount of indentation, the required load for a square plate must be greater than for a circular plate. Accordingly, a square plate is stiffer than a circular plate in indentation.

CONCLUSIONS

Three-dimensional contact problems of isotropic square plates indented by a rigid spherical indentor were solved by combining an analytical elasticity approach with a numerical procedure. The approach employed the exact solution technique developed by

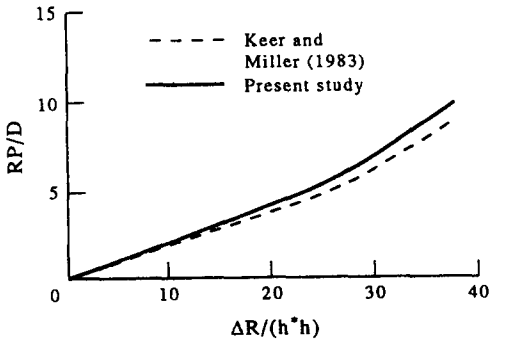

Fig. 14. Load vs indentor displacement.

Pagano (1970) in conjunction with the Point Matching (PM) method of Sun and Sankar (1983) and enhanced by the Redundant Field Point (RFP) method presented by Singh and Paul (1974) to overcome the inherent numerical sensitivity due to the ill-posed nature of the problem.

For small indentations, the results indicated a Hertzian type behavior and were identical to the circular plate solutions obtained by Keer and Miller (1983a). However, a comparatively limited range of applicability of Hertzian type solutions were revealed with respect to the limit of the validity of a circular contact area. For comparatively large indentations, the determination of the contact area was based on the consideration of the geometry of the structure and was found to be a hypotrocoid of four lobes. In summary, the proposed boundary geometry caused a reduction of the contact length along the through-the-corner direction as the indentation proceeded. In this direction, the peak contact stress was less in magnitude than for the circular plate solution. However, in the through-the-mid-span directions, the magnitude of peak contact stress was appreciably greater than that of the circular plate. The load versus indentor displacement relation indicated that a square plate is stiffer in indentation than a circular plate with a diameter which is equal to the edge length of the square plate.

Acknowledgement—The authors would like to express their sincere appreciation to Professor C. W. Smith for his valuable technical suggestion during the course of this study.

REFERENCES

Ahmadi, N., Keer, L. M. and Mura, T. (1983). Non-Hertzian contact stress analysis for an elastic half space-normal and sliding contact. *Int. J. Solids Structures* **19,** 357–373.

Chen, C. F. (1991). Contact of orthotropic laminates with a rigid spherical indentor. Ph.D. Dissertation, Virginia Polytechnic Institute and State University, Blacksburg, Virginia.

Duffek, W. (1983). Contact geometry in wheel rail vehicles. In *Contact Mechanics and Wear of Rail/Wheel Systems* (Edited by J. Kalousek, R. V. Durripati and G. M. L. Gladwell), pp. 161–181. University of Waterloo Press, Waterloo, Canada.

Duffek, W. and Jaschinski, A. (1981). Efficient implementation of wheel–rail contact mechanics in dynamic curving. *Proc. 7th IAVSD Symposium on the Dynamics of Vehicles on Roads and Tracks.* Cambridge, U.K.

Hartnett, M. J. (1980). A general numerical solution for elastic body contact problems. *Proc. Symposium on Solid Contact and Lubrication*, AMD-Vol. **39,** pp. 51–66.

Kalker, J. J. (1979). Survey of wheel–rail rolling contact theory. *Veh. Syst. Dyn.* **8,** 317–350.

Kalker, J. J. (1980a). Review of wheel–rail contact theories. *Proc. Symposium on the General Problem of Rolling Contact*, AMD-Vol. 40, pp. 66–92.

Kalker, J. J. (1980b). Numerical contact elastostatics. In *Variational Methods in the Mechanics of Solids* (Edited by S. Nemat-Nasser), pp. 242–248. Pergamon Press, Oxford.

Kalker, J. J. (1981). The numerical calculation of the contact problem in the theory of elasticity. In *Non-linear Finite Element Analysis in Structural Mechanics* (Edited by W. Wunderlich, E. Stern and K.-J. Bathe), pp. 637–653. Springer, New York.

Kalker, J. J. (1983). Two algorithms for the contact problem in elastostatics. In *Contact Mechanics and Wear of Rail/Wheel Systems* (Edited by J. Kalousek, R. V. Durripati and G. M. L. Gladwell), pp. 103–120. University of Waterloo Press, Waterloo, Canada.

Keer, L. M. and Ballarini, R. (1983). Smooth contact between a rigid indenter and an initially stressed orthotropic beam. *AIAA Jl* **21,** 1035–1042.

Keer, L. M. and Miller, G. R. (1983a). Contact between an elastically supported circular plate and a rigid indenter. *Int. J. Engng Sci.* **21,** 681–690.

Keer, L. M. and Miller, G. R. (1983b). Smooth indentation of finite layer. *J. Engng Mech.* **109,** 706–717.

Keer, L. M. and Schonberg, W. P. (1986). Smooth indentation of an isotropic cantilever beam. *Int. J. Solids Structures* **22,** 87–106.

Pagano, N. J. (1970). Exact solutions for rectangular bidirectional composites and sandwich plates. *J. Composite Mater.* **4,** 20–34.

Paul, B. and Hashemi, J. (1979). An improved numerical method and computer program for counterformal contact stress problems. In *Computational Techniques for Interface Problems* (Edited by K. C. Park and D. K. Gartlung), AMD-Vol. 30, pp. 165–180.

Paul, B. and Hashemi, J. (1980a). Contact pressures on closely conforming elastic bodies. *Proc. of Symposium on Solid Contact and Lubrication*, AMD-Vol. 39, pp. 67–78.

Paul, B. and Hashemi, J. (1980b). Contact geometry associated with arbitrary rail and wheel profiles. *Proc. of Symposium on the General Problem of Rolling Contact*, AMD-Vol. 40, pp. 93–105.

Sankar, B. V. and Sun, C. T. (1983). Indentation of a beam by a rigid cylinder. *Int. J. Solids Structures* **19,** 293–303.

Schonberg, W. P., Keer, L. M. and Woo, T. K. (1987). Low velocity impact of transversely isotropic beams and plates. *Int. J. Solids Structures* **23,** 871–896.

Singh, K. P. and Paul, B. (1974). Numerical solution of non-Hertzian elastic contact problems. *J. Appl. Mech.* **41,** 484–490.

Sun, C. T. and Sankar, B. V. (1985). Smooth indentation of an initially stressed orthotropic beam. *Int. J. Solids Structures* **21,** 161–176.

APPENDIX: EXPRESSIONS FOR THE T_{nm}s IN EQN (11)

For $k+l \neq K+1$,

$$T_{nm} = \frac{16}{\pi^2 pqL^2} \cos(px_{k+1}) \cos(qy_{l+1}). \tag{A1}$$

For $k = 1, l = K$,

$$T_{nm} = \frac{J_{nm}}{q}\left[\frac{1}{p}\sin(px'_2)\sin(qy'_K) + \frac{t_2}{p^2 - t_2^2}[\cos(t_1) - \cos(px'_2)]\right], \tag{A2}$$

where

$$t_1 = qm_1 x'_2, \quad t_2 = qm_1, \quad m_1 = \frac{y_{K+1} - y_K}{x'_2}.$$

For $k = K, l = 1$,

$$T_{nm} = \frac{J_{nm}}{p}\left[\frac{1}{q}\sin(px'_K)\sin(qy'_2) + \frac{t_2}{q^2 - t_2^2}[\cos(t_1) - \cos(qy'_2)]\right], \tag{A3}$$

where

$$t_1 = pm_1 y'_2, \quad t_2 = pm_1, \quad m_1 = \frac{x_{K+1} - x_K}{y'_2}.$$

For $k+l = K+1$; $k = 2, 3, \ldots, K-1$;

$$T_{nm} = J_{nm}\left[\frac{1}{pq} f_{s(k,K+2-k)} + \frac{\frac{p}{q}F_{S(k)} - m_1 F_{C(k)}}{p^2 - (m_1 q)^2}\right], \tag{A4}$$

where

$$F_{S(k)} = [f_{s(k+1,K+1-k)} - f_{s(K,K+2-k)}], \quad F_{C(k)} = [f_{c(K+1,K+1-k)} - f_{c(k,K+2-k)}],$$

$$f_{s(k,l)} = \sin(px'_k)\sin(qy'_l), \quad f_{c(k,l)} = \cos(px'_k)\cos(qy'_l), \quad J_{nm} = \frac{16(-1)^{n+m}}{L^2}.$$

In the above

$$p = \frac{n\pi}{L}, \quad q = \frac{m\pi}{L}, \quad x'_i = x_i - \frac{L}{2}, \quad y'_i = y_i - \frac{L}{2} \quad \text{and} \quad i = 1, 2, \ldots, K+1.$$